Inorg. Chem. **2009**, *48*, 3205−3214

Synthesis, Structure, and Catalase-Like Activity of Dimanganese(III) Complexes of 1,5-Bis[(2-hydroxy-5-X-benzyl)(2-pyridylmethyl)amino]-pentan-3-ol (X = H, Br, OCH_3)

Hernán Biava,[†] Claudia Palopoli,[†] Carine Duhayon,[‡] Jean-Pierre Tuchagues,[‡] and Sandra Signorella*[,†]

Instituto de Química Rosario - CONICET, Universidad Nacional de Rosario, Suipacha 531, S2002LRK Rosario, Argentina, and Laboratoire de Chimie de Coordination, UPR CNRS 8241, 205 Route de Narbonne, 31077 Toulouse Cedex 04, France

Received October 16, 2008

New diMn^{III} complexes of general formula $[Mn_2L(\mu\text{-OR})(\mu\text{-OAc})]BPh_4$ (H_3L = 1,5-bis[(2-hydroxy-5-X-benzyl)(2-pyridylmethyl)amino]pentan-3-ol, **1**: X = H, R = Me, **2**: X = OMe, R = Me, **3**: X = Br, R = Me, **4**: X = Br, R = Et) have been prepared and structurally characterized. The synthesized complexes possess a triply bridged $(\mu\text{-alkoxo})_2(\mu\text{-acetato})Mn_2^{3+}$ core, a short intermetallic distance of 2.95/6 Å modulated by the aliphatic spacers between the central alcoholato and *N*-amino donor sites, and the remaining coordination sites of the two Mn^{III} centers occupied by the six donor atoms of the polydentate ligand. In dimethylformamide, complexes **1**−**3** are able to disproportionate more than 1500 equiv of H_2O_2 without significant decomposition, with first-order dependence on catalyst and saturation kinetic on $[H_2O_2]$. Spectroscopic monitoring of the reaction mixtures revealed that the catalyst converts into $[Mn_2^{III}(\mu\text{-O})(\mu\text{-OAc})L]$, which is the major active form during cycling. Overall, kinetics and spectroscopic studies of H_2O_2 dismutation by these complexes converge at a catalytic cycle between Mn^{III}_2 and Mn^{II}_2 oxidation levels. Comparison to other alkoxo-bridged complexes suggests that the binding mode of peroxide to the metal center of the Mn^{III}_2 form of the catalyst is a key factor for tuning the Mn oxidation states involved in the H_2O_2 dismutation mechanism.

Introduction

Manganese is present in the active site of many enzymes involved in biological redox processes and plays an important role in the metabolism of dioxygen and its reduced forms.[1] Among the Mn redox enzymes, manganese catalases effectively catalyze the disproportionation of harmful H_2O_2 into H_2O and O_2 by using a $Mn_2(\mu\text{-}O_2CR)(\mu\text{-O/OH/}H_2O)_2$ structural unit as the active site.[2,3] The catalytic cycle is known to involve a redox transformation between Mn^{II}_2 and Mn^{III}_2 but the mechanism is still poorly understood.[4−6] Because of the potential use as catalytic scavengers of H_2O_2 for preventing oxidative stress injuries, a large number of dimanganese complexes involving different types of ligands and Mn oxidation states have been synthesized and characterized in an attempt to mimic the catalytic activity of the enzyme.[7−15] However, the best functional models are still

* To whom correspondence should be addressed. E-mail: signorel@infovia.com.ar.
[†] Instituto de Química Rosario.
[‡] Laboratoire de Chimie de Coordination du CNRS.

(1) Larson, E. J.; Pecoraro, V. L. In *Manganese Redox Enzymes*; Pecoraro, V. L. , Ed.; VCH Publishers, Inc.: New York, 1992; pp 1−28.
(2) Antonyuk, S. V.; Barynin, V. V. *Crystallogr. Rep.* **2000**, *45*, 105–116.
(3) Barynin, V. V.; Whittaker, M. M.; Antonyuk, S. V.; Lamzin, V. S.; Harrison, P. M.; Artymiuk, P. J.; Whittaker, J. W. *Structure* **2001**, *9*, 725–738.
(4) Dismukes, G. C. *Chem. Rev.* **1996**, *96*, 2909–2926.
(5) Waldo, G. S.; Penner-Hahn, J. E. *Biochemistry* **1995**, *34*, 1507–1512.
(6) Yoder, D. W.; Hwang, J.; Penner-Hahn, J. E. In *Metal Ions in Biological Systems*; Sigel, A., Sigel, H., Eds.; Marcel Dekker Inc.: New York, 1999; Vol. 37, p 535.
(7) Wu, A. J.; Penner-Hahn, J. E.; Pecoraro, V. L. *Chem. Rev.* **2004**, *104*, 903–938.
(8) Godbole, M. D.; Kloskowski, M.; Hage, R.; Rompel, A.; Mills, A. M.; Spek, A. L.; Bouwman, E. *Eur. J. Inorg. Chem.* **2005**, 305–313.
(9) Dubois, L.; Xiang, D. F.; Tan, X. S.; Latour, J. M. *Eur. J. Inorg. Chem.* **2005**, 1565–1571.
(10) Biava, H.; Palopoli, C.; Shova, S.; De Gaudio, M.; Daier, V.; González-Sierra, M.; Tuchagues, J.-P.; Signorella, S. *J. Inorg. Biochem.* **2006**, *100*, 1660–1671.
(11) Moreno, D.; Palopoli, C.; Daier, V.; Shova, S.; Vendier, L.; González Sierra, M.; Tuchagues, J.-P.; Signorella, S. *Dalton Trans.* **2006**, 5156–5166.
(12) De Boer, J. W.; Browne, W. R.; Feringa, B. L.; Hage, R. C. R. *Chimie* **2007**, *10*, 341–354.

10.1021/ic8019793 CCC: $40.75
Published on Web 03/09/2009

several orders of magnitude slower than catalase enzymes in terms of k_{cat} and k_{cat}/K_M.[16] This limitation stimulates the interest in establishing structure/activity relationships to afford mechanistic insight into the catalysis of H_2O_2 disproportionation.

The highly efficient dismutation of H_2O_2 by manganese catalases requires a two-electron redox cycle that involves Mn^{II}_2/Mn^{III}_2 oxidation levels. Thus, the fine-tuning of Mn redox states is a critical feature when using artificial compounds to model the enzymatic activity.[4] Mechanistic studies of H_2O_2 dismutation performed on diMn complexes including polydentate ligands with a central bridging alcoholato[10,11,16−23] or phenolato[9,24−26] have shown that, depending upon the Mn···Mn separation and Mn coordination environment, either Mn^{II}_2/Mn^{III}_2, $Mn^{II}Mn^{III}/Mn^{III}Mn^{IV}$, or Mn^{III}_2/Mn^{IV}_2 couples are involved in the catalysis. The redox couples of these complexes fall within the same range of potentials, so that there must be other factors that modulate Mn redox states during catalysis. With the aim of gaining new insights on the structural features that control the Mn oxidation states involved in the catalase activity, we report here the synthesis, structure, properties, and catalase-like activity of new alkoxo-bridged diMn complexes that combine short (<3.0 Å) Mn···Mn separation and metal coordination sphere saturated by non-labile donors: $[Mn_2L^{1-3}(\mu\text{-OAc})(\mu\text{-OR})]BPh_4$ (R = Me or Et), obtained with the heptadentate ligand 1,5-bis[(2-hydroxybenzyl)(2-piridylmethyl)amino]pentan-3-ol (H_3L^1) and two phenyl-ring substituted derivatives (5-methoxy (H_3L^2) and 5-bromo (H_3L^3)), and compare their catalytic activity with that of other alkoxo-bridged diMn complexes. The present study adds support to the proposal that the binding mode of peroxide to the $diMn^{III}$ center is a critical feature for determining the Mn oxidation states involved in the catalytic cycle.

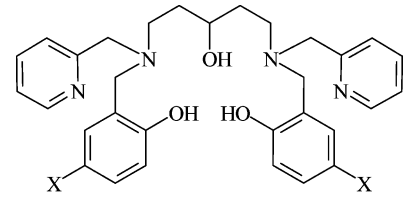

H_3L^1: X = H; H_3L^2: X = OMe; H_3L^3: X = Br

Experimental Section

Materials. All reagents or AR chemicals were used as purchased. Solvents were purified by standard methods. The concentration of H_2O_2 stock solution was determined by iodometric titration.

Synthesis of Ligands. 1,5-Bis[(2-hydroxybenzyl)(2-pyridylmethyl)amino]pentan-3-ol (H_3L^1), 1,5-bis[(2-hydroxy-5-methoxybenzyl)(2-pyridylmethyl)amino]pentan-3-ol (H_3L^2), and 1,5-bis[(5-bromo-2-hydroxybenzyl)(2-pyridylmethyl)amino]pentan-3-ol (H_3L^3) were prepared through a synthetic procedure slightly modified from that published for similar ligands.[27] Condensation of 5 mmol of 1,5-diaminopentan-3-ol[28] with 2 equiv of the corresponding salicylaldehyde in 20 mL of ethanol yielded the corresponding Schiff-base as a yellow solid. The Schiff-base was reduced in situ with $NaBH_4$ (3 equiv), added carefully in small amounts, and then heated at 60 °C during 30 min. The resulting solution was stirred for 1 day, and then treated with concentrated HCl to reach pH 6, and 4 M NaOH up to pH 10. Precipitated sodium borate was filtered off, and the filtrate was added to 20 mL of an aqueous solution of previously neutralized 2-pyridylmethyl choride hydrochloride (2 equiv). The reaction mixture was heated at 70 °C during 5 h. Over this period, 4 M NaOH was added in small portions so that the pH never exceeded 10. The reaction mixture was then stirred overnight. The 5 h preheating of the mixture shortened the reaction time from 5 days (without heating) to 1 day. The red solution was cooled to room temperature, extracted with chloroform (3 × 20 mL), and the organic phase was dried over $MgSO_4$. Evaporation of the solvent yielded the H_3L^{1-3} ligands as red residues. The ligands were characterized by ^{1}H NMR, IR, and electrospray ionization mass spectrometry (ESI-MS) and were used without further purification.

H_3L^1. Yield 22.36%. ^{1}H NMR ($CDCl_3$) δ: 8.5 (m, 2H, py), 7.7−6.6 (m, 14 H, ph and py), 3.9−3.5 (m, 9H, N−C$\underline{H}_2$-ph, N−C$\underline{H}_2$-py, $\underline{H}$-C(OH)-), 2.7 (m, 4H, -C$\underline{H}_2$-N), 1.6 (m, 4H, (HO)C−C$\underline{H}_2$-). Significant IR bands (KBr,νcm^{-1}): 3380, 3210 (broad), 3060, 2940, 2840, 1593, 756. ESI-MS (CH_3CN): m/z = 513.65 $[H_4L^1]^+$.

H_3L^2. Yield 21.15%. ^{1}H NMR ($CDCl_3$) δ: 8.55 (m, 2H, py protons), 7.7−6.5 (m, 12 H, ph and py), 4−3.6 (m, 9H, N−C$\underline{H}_2$-ph, N−C$\underline{H}_2$-py, $\underline{H}$-C(OH)-), 3.72 (s, 6H, -OCH_3), 2.75 (m, 4H, -C$\underline{H}_2$-N), 1.6 (m, 4H, (HO)C−C$\underline{H}_2$-). Significant IR bands (KBr,ν cm^{-1}): 3250 (broad), 3060, 2933, 2833, 1593, 1250, 810, 759. ESI-MS (CH_3CN): m/z = 573.70 $[H_4L^2]^+$.

H_3L^3. Yield 21.00%. ^{1}H NMR ($CDCl_3$) δ: 8.5 (m, 2H, py protons), 7.8−6.6 (m, 12 H, ph and py), 4−3.5 (m, 9H, N−C$\underline{H}_2$-ph, N−C$\underline{H}_2$-py, $\underline{H}$-C(OH)-), 2.7 (m, 4H, -C$\underline{H}_2$-N), 1.55 (m, 4H, (HO)C−C$\underline{H}_2$-). Significant IR bands (KBr,νcm^{-1}): 3350 (broad), 3060, 2930, 2835, 1594, 817, 757, 734. ESI-MS (CH_3CN): m/z = 671.11 $[H_4L^3]^+$.

Synthesis of Complexes. $[Mn_2L^1(\mu\text{-OMe})(\mu\text{-OAc})]BPh_4$ (1). $Mn(OAc)_3.2H_2O$ (0.48 g, 1.80 mmol) was added to a solution of H_3L^1 (0.46 g, 0.9 mmol) in methanol (25 mL). The mixture was

(13) Singh, U. P.; Tyagi, P.; Upreti, S. *Polyhedron* **2007**, *26*, 3625–3632.
(14) Shin, B. K.; Kim, Y.; Kim, M.; Han, J. *Polyhedron* **2007**, *26*, 4557–4566.
(15) Dubois, L.; Pécaut, J.; Charlot, M. F.; Baffert, C.; Collomb, M. N.; Deronzier, A.; Latour, J. M. *Chem.—Eur. J.* **2008**, *14*, 3013–3025.
(16) Signorella, S.; Rompel, A.; Buldt-Karentzopoulos, K.; Krebs, B.; Pecoraro, V. L.; Tuchagues, J.-P. *Inorg. Chem.* **2007**, *46*, 10864–10868.
(17) Palopoli, C.; Chansou, B.; Tuchagues, J.-P.; Signorella, S. *Inorg. Chem.* **2000**, *39*, 1458–1462.
(18) Palopoli, C.; González-Sierra, M.; Robles, G.; Dahan, F.; Tuchagues, J.-P.; Signorella, S. *J. Chem. Soc., Dalton Trans.* **2002**, 3813–3819.
(19) Daier, V.; Biava, H.; Palopoli, C.; Shova, S.; Tuchagues, J.-P.; Signorella, S. *J. Inorg. Biochem.* **2004**, *98*, 1806–1817.
(20) Signorella, S.; Tuchagues, J.-P.; Moreno, D.; Palopoli, C. In *Inorganic Biochemistry Research Progress*; Hughes, J. G., Robinson, A. J., Eds.; Nova Sci. Publ. Inc.: New York, 2008; pp 243−279.
(21) Velasco, A.; Bensiek, S.; Pecoraro, V. L. *Inorg. Chem.* **1998**, *37*, 3301–3309.
(22) Pessiki, P. J.; Dismukes, G. C. *J. Am. Chem. Soc.* **1994**, *116*, 898–903.
(23) Boelrijk, A. E. M.; Dismukes, G. C. *Inorg. Chem.* **2000**, *39*, 3020–3028.
(24) Okawa, H.; Sakiyama, H. *Pure Appl. Chem.* **1995**, *67*, 273–280.
(25) Sakiyama, H.; Okawa, H.; Isobe, R. *J. Chem. Soc., Chem. Commun.* **1993**, 882–884.
(26) Dubois, L.; Caspar, R.; Jacquamet, L.; Petit, P. E.; Charlot, M. F.; Baffert, C.; Collomb, M. N.; Deronzier, A.; Latour, J. M. *Inorg. Chem.* **2003**, *42*, 4817–4827.
(27) Krebs, B.; Schepers, K.; Bremer, B.; Henkel, G.; Althous, E.; Warmuth, W.; Griesar, K.; Haase, W. *Inorg. Chem.* **1994**, *33*, 1907–1914.
(28) Murase, I.; Hatano, M.; Tanaka, M.; Ueno, S.; Okawa, H.; Kida, S. *Bull. Chem. Soc. Jpn.* **1982**, *55*, 2404–2408.

stirred for 20 min, and the resulting brown solution was filtered. A methanol solution of $NaBPh_4$ (0.31 g, 0.9 mmol) was then added, and the reaction mixture was stirred for 24 h. A green microcrystalline precipitate formed, which was collected by filtration, washed with cold methanol, and dried under vacuum. Yield: 0.52 g (0.5 mmol, 28%). Anal. Calcd for $C_{58}H_{59}BMn_2N_4O_6$: C 67.71, H 5.78; N 5.45; Mn 10.68, B 1.05. Found: C 69.23; H 5.70; N 5.52; Mn 9.09; B 1.16. Molar conductivity = 104 Ω^{-1} cm^2 M^{-1}. ESI-MS: m/z = 709 [**1** − BPh_4]$^+$. Significant IR bands (KBr,νcm^{-1}): ν_{CH} 3056, 3033, 3000, 2985, 2924, 2858, $\nu_{Ar,Py}$ 1604, 1574, ν_{CO2}- 1544/1427, $\nu_{CH\ Ar/Py\ out\text{-}of\text{-}plane}$ 829, 760, 735, 707. UV−vis λ nm (ε M^{-1} cm^{-1}) in dimethylformamide (DMF): 450 (sh), 645 (570).

[Mn_2L^2(μ-OMe)(μ-OAc)]BPh_4 (2). Following the same procedure as for **1**, H_3L^2 (0.64 g, 1.12 mmol) afforded 0.32 g of **2** (0.30 mmol, 26%). Anal. Calcd for $C_{60}H_{63}BMn_2N_4O_8$: C 66.17, H 5.79; N 5.14; Mn 10.11; B 1.01. Found: C 66.89; H 5.79; N 4.82; Mn 10.11; B 0.80. Molar conductivity = 124 Ω^{-1} cm^2 M^{-1}. ESI-MS: m/z = 769 [**2** − BPh_4]$^+$. Significant IR bands (KBr,νcm^{-1}): ν_{CH} 3057, 3034, 2930, 2986, 2833, $\nu_{Ar,Py}$ 1604, 1573, ν_{CO2}- 1545/1426, $\nu_{CH\ Ar/Py\ out\text{-}of\text{-}plane}$ 845, 813, 760, 745, 734, 707. UV−vis λ_{max} nm (ε M^{-1} cm^{-1}) in DMF: 295 (9700), 390 (sh), 665 (650).

[Mn_2L^3(μ-OMe)(μ-OAc)]$BPh_4\cdot 2H_2O$ (3). Following the same procedure as for **1**, H_3L^3 (0.66 g, 0.9 mmol) afforded 0.40 g of **3**$\cdot 2H_2O$ (0.33 mmol, 36,4%). Anal. Calcd for $C_{58}H_{57}BBr_2Mn_2N_4O_6\cdot 2H_2O$: C 56.98, H 5.03; N 4.58; Br 13.07; Mn 8.97; B 0.88. Found: C 56.43; H 4.32; N 4.36; Br 13.03; Mn 9.13; B 0.90. Molar conductivity = 123 Ω^{-1} cm^2 M^{-1}. ESI-MS: m/z = 867 [**3** − BPh_4]$^+$. Significant IR bands (KBr,νcm^{-1}): ν_{OH} 3436, ν_{CH} 3055, 2989, 2925, 2852, $\nu_{Ar,Py}$ 1604, 1577, ν_{CO2}- 1542/1418, $\nu_{CH\ Ar/Py\ out\text{-}of\text{-}plane}$ 820, 796, 760, 752, 734, 707. UV−vis λ nm (ε M^{-1} cm^{-1}) in DMF: 290 (sh), 380 (sh), 630 (846). The content of 2 molecules of noncoordinated water was confirmed by thermogravimetric analysis of the complex which showed a 2.9% mass loss at 120 °C. Single crystals of **[MnL^3(μ-OEt)(μ-OAc)]$BPh_4\cdot 0.75CHCl_3\cdot 1.5H_2O$** (**4**) suitable for X-ray diffraction were obtained from a solution of **3** in a 1:1 $CHCl_3$/EtOH mixture upon standing in air for several days.

Physical Measurements. Electronic spectra were recorded on a JASCO V550 spectrophotometer with thermostatted cell compartments. IR spectra were recorded on a Perkin-Elmer Spectrum One FT-IR spectrophotometer. ESI-mass spectra were recorded on a Perkin-Elmer SCIEX 365 LCMSMS mass spectrometer, using $\sim 10^{-5}$ M solutions of the complexes or ligands in CH_3CN at a flow rate of 5 μL min^{-1}. DMF reaction mixtures were diluted with CH_3CN to a $\approx 10^{-5}$ M concentration. Electron paramagnetic resonance (EPR) spectra were obtained on a Bruker ESP 300 E spectrometer with a microwave frequency generated with a Bruker ER 04 (9−10 GHz). The microwave frequencies were measured with a Racal-Dana frequency meter, and the magnetic field was measured with a Bruker NMR probe Gaussmeter. ^{1}H NMR spectra were acquired on a Bruker AVANCE II 600 NMR spectrometer at ambient probe temperature (ca. 26 °C), with nominal operating frequency of 600.13 MHz, using super WEFT sequence, with acquisition time of 23 ms. Conductivity measurements were performed using a Horiba D24 conductivity meter, on 1.0 mM solutions of the complexes in 1:1 methanol/CH_3CN mixtures. The electrochemical experiments were performed with a computer-controlled Princeton Applied Research potentiostat, model VERSASTAT II, with model 270/250 Research Electrochemistry Software. Studies were carried out under Ar, in DMF or CH_3CN solutions using 0.1 M Bu_4NPF_6 as supporting electrolyte and $\sim 10^{-3}$ M of the complex. The working electrode was a Pt wire, and the reference electrode was Ag/AgCl with Pt as the auxiliary electrode. All potentials are referred to the Ag/AgCl electrode. When the described conditions are used, the ferrocene/ferrocenium redox couple was observed at $E_{1/2}$ = 396 mV in CH_3CN and $E_{1/2}$ = 481 mV in DMF.

Volumetric Measurements. The stoichiometry of the reaction was measured by volumetric determination of the evolved O_2 from reaction mixtures in DMF, CH_3CN, or methanol as previously described.[17]

Kinetic Measurements. Oxygen evolution studies were carried out polarographically using a Clark-type oxygen electrode with an YSI oxygen-monitoring system (Model 5300, Yellow Springs Instruments Co., Inc.). The initial rate method was used to determine the rate constants (see reference 17 for further details). Each rate constant reported here represents the mean value of multiple determinations that fall within ±5%. Experiments were carried out at 10 °C. The solubility of oxygen in air-saturated solution of DMF was determined by a modified Winkler method.[29] The O_2 concentration measured in DMF equilibrated with air (20.9% O_2) at 1 atm and 283 K was 1.47 ± 0.01 mM.

X-ray Crystal Structure Determination. Crystallographic data for compound [MnL^3(μ-OEt)(μ-OAc)]$BPh_4\cdot 0.75CHCl_3\cdot 1.5H_2O$ were collected at 180 K on an Oxford-Diffraction XCALIBUR CCD Diffractometer equipped with a Cryojet cooler device from Oxford Instruments and a graphite-monochromated Mo-Kα radiation source. The unit cell determination and data integration were carried out using the CrysAlis package.[30] The structure was solved using SIR 92[31] and refined by full-matrix least-squares on F_o with CRYSTALS.[32] Mn and Br atoms were refined with anisotropic displacement parameters. Owing to the poor quality of collected data, B, C, N, O, and Cl atoms could be refined only with isotropic displacement parameters. Moreover, to reduce the number of free parameters, the BPh_4 anions were refined as rigid groups. H atoms were treated as riding on their parent atom with fixed displacement parameters (1.2−1.5 times U_{eq} of the parent atom). Hydrogen atoms of water molecules could not be located. Absorption corrections were applied using Multiscan.[33] The molecular plot was drawn with Cameron.[34] Crystal data collection and refinement parameters are summarized in Table 1.

Results

Characterization of Complexes 1−4. Crystal Structure of [MnL^3(μ-OEt)(μ-OAc)]$BPh_4\cdot 0.75CHCl_3\cdot 1.5H_2O$ (4$\cdot$ **$0.75CHCl_3\cdot 1.5H_2O$).** Efforts to obtain single crystals of complexes **1**−**3** by recrystallization from methanol, DMF, or CH_3CN were unsuccessful. Several green needles of **4** obtained from a solution of **3** in an 1:1 EtOH/$CHCl_3$ mixture were used for the X-ray diffraction study, and the best set of collected data was used to solve the structure. Despite the poor structural resolution, the main features of the molecular structure of **4** are clearly established. The asymmetric unit consists of two crystallographically independent diMn complex cations, non-coordinated Ph_4B^- anions, solvate water, and $CHCl_3$ molecules in a molar ratio 1:1:0.75:1.5. The molecular structure of complex **4** is illustrated in

(29) James, H. J.; Broman, R. F. *Anal. Chim. Acta* **1969**, *48*, 411–417.
(30) *CrysAlis RED, version 1.70*, Oxford Diffraction Ltd.: Oxford, U.K., 2002.
(31) Altomare, A.; Cascarano, G.; Giaccovazzo, C.; Guagliardi, A.; Burla, M. C.; Polidori, G.; Camalli, M. *J. Appl. Crystallogr.* **1994**, *27*, 435.
(32) Betteridge, P. W.; Carruthers, J. R.; Cooper, R. I.; Prout, K.; Watkin, D. J. *J. Appl. Crystallogr.* **2003**, *36*, 1487.
(33) Blessing, R. H. *Acta Crystallogr.* **1995**, *51*, 33.
(34) Watkin, D. J.; Prout, C. K.; Pearce, L. J. *CAMERON*; Chemical Crystallography Laboratory, University of Oxford: Oxford, U.K., 1996.

Table 1. Summary of Crystal Data for **4**·0.75$CHCl_3$·1.5H_2O

empirical formula	$C_{59}H_{59}Br_2BMn_2N_4O_6(CHCl_3)_{0.75}(H_2O)_{1.5}$
M	1317.17
temperature, K	180
wavelength, Å	0.71073
crystal system, space group	triclinic, $P\bar{1}$
a, Å	10.971(2)
b, Å	23.169(4)
c, Å	25.272(4)
α, deg	75.590(10)
β, deg	78.68(2)
γ, deg	76.840(10)
V, Å^3	5991.6(18)
Z	4
$\rho_{(calcd.)}$, Mg/m^3	1.46
μ_{Mo}, mm^{-1}	1.91
$F(000)$	2678
crystal size, mm	0.5 × 0.06 × 0.03
θ range, deg	2.720−29.070
index ranges	$-11 \le h \le 14$, $-31 \le k \le 31$, $-34 \le l \le 34$
no. of reflections:	
measured	31298
unique ($I > 2\sigma(I)$)	3667
no. of refined parameters	518
GOF for F^2	1.1353
[a] R [$I > 2\sigma(I)$]	0.0973
[b] wR	0.0956

[a] $R = \sum||F_o| - |F_c||/\sum|F_o|$. [b] $wR = \{\sum[w(F_o^2 - F_c^2)^2]/\sum w(F_o^2)^2\}^{1/2}$.

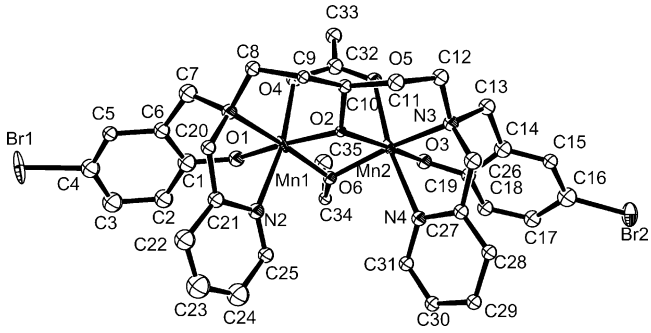

Figure 1. Oak Ridge Thermal Ellipsoid Plot (ORTEP) diagram of the cation $[Mn_2L^3(\mu\text{-OEt})(\mu\text{-OAc})]^+$ (**4**). The thermal ellipsoids are drawn at the 30% probability level. Hydrogen atoms have been omitted for clarity.

Figure 1, and relevant bond lengths and angles are collected in Table 2. In each complex cation, $L^{3(3-)}$ acts as a heptadentate ligand through the N_4O_3 donor set. The two Mn atoms are six-coordinated and triply bridged by the central alcoholato of $L^{3(3-)}$, and exogenous *syn,syn*-acetato and ethanolato ligands. The phenolato-*O*, amino-*N* and alcoholato-*O* atoms of the ligand and the ethanolato-*O* donor atom form a meridional geometry around each Mn. One of the axial positions of each Mn atom is occupied by an acetato-*O* atom, and the other one is occupied by the pyridyl-*N* atom of $L^{3(3-)}$. The Mn−N/O bond lengths are typical of the Mn^{III} oxidation state.[35−38] The coordination polyhedra of the Mn centers may be described as elongated octahedra, with the axial Mn−O/N bonds distances (Mn−N_{py} av. 2.26 Å, Mn−O_{ac} av. 2.15 Å) distinctly longer than the equatorial Mn−N/O ones (av. 1.97 Å), clear signature of Jahn−Teller distorted co-ordination sphere of Mn^{III} ions. The values of the *trans*-angles in the coordination environment of each Mn ion are in the range of 167−172° (Table 2) indicating distortion from a pure octahedral geometry. The Mn···Mn separation (2.95/6 Å) and the Mn−O−Mn angles (98.2−98.6°) defining the core of the asymmetric unit are similar to those found in triply bridged bis(μ-alkoxo)(μ-carboxylato) diMn^{III} complexes of the X-salpentOH (salpentOH = 1,5-bis(salicylideneamino)pentan-3-ol) family, which also bear the 3-pentanol backbone and possess axial elongation perpendicular to the bridging plane.[10,11,17−19] This intermetallic distance is shorter than that of Mn^{III}_2 complexes of polydentate ligands derived from 1,3-diaminopropan-2-ol (≈3.2 Å), either with bis(μ-alkoxo), bis(μ-alkoxo)(μ-carboxylato), or bis(μ-acetato)(μ-alkoxo) bridging motifs, which possess a Jahn−Teller elongation axis oriented along the bridging core.[36,38−41] These results suggest that the length of the spacers between the central *O*-alkoxo and the *N*-donor groups modulates the Mn···Mn separation in the resulting Mn^{III}_2 complexes, independently of the bridging motif.

Table 2. Selected Bond Lengths (Å) and Angles (deg) for Complex **4**·0.75$CHCl_3$·1.5H_2O

Bond Lengths			
Mn(1)−N(1)	2.17(2)	Mn(3)−N(5)	2.15(2)
Mn(1)−N(2)	2.26(2)	Mn(3)−N(6)	2.24(2)
Mn(1)−O(1)	1.821(19)	Mn(3)−O(7)	1.852(17)
Mn(1)−O(2)	1.940(17)	Mn(3)−O(8)	1.966(17)
Mn(1)−O(4)	2.148(19)	Mn(3)−O(10)	2.133(19)
Mn(1)−O(6)	1.920(18)	Mn(3)−O(12)	1.926(19)
Mn(2)−N(3)	2.12(2)	Mn(4)−N(7)	2.14(2)
Mn(2)−N(4)	2.30(2)	Mn(4)−N(8)	2.24(3)
Mn(2)−O(2)	1.974(16)	Mn(4)−O(8)	1.923(18)
Mn(2)−O(3)	1.857(18)	Mn(4)−O(9)	1.855(19)
Mn(2)−O(5)	2.11(2)	Mn(4)−O(11)	2.200(18)
Mn(2)−O(6)	1.988(18)	Mn(4)−O(12)	1.964(18)
Angles			
N(1)−Mn(1)−O(6)	172.0(8)	N(5)−Mn(3)−O(12)	170.3(8)
N(2)−Mn(1)−O(4)	170.0(8)	N(6)−Mn(3)−O(10)	170.0(8)
O(1)−Mn(1)−O(2)	171.5(8)	O(7)−Mn(3)−O(8)	171.6(8)
N(3)−Mn(2)−O(6)	166.9(8)	N(7)−Mn(4)−O(12)	171.3(8)
N(4)−Mn(2)−O(5)	170.5(8)	N(8)−Mn(4)−O(11)	170.2(9)
O(2)−Mn(2)−O(3)	170.7(8)	O(8)−Mn(4)−O(9)	171.0(8)
Mn(1)−O(2)−Mn(2)	98.2(7)	Mn(3)−O(8)−Mn(4)	98.6(8)
Mn(1)−O(6)−Mn(2)	98.4(8)	Mn(3)−O(12)−Mn(4)	98.5(8)

FT-IR Spectroscopy. Comparison of the IR spectra of **1**−**4** evidences the "fingerprint" pattern of $L^{1-3(3-)}$ coordinated to the Mn ions and confirms their analogous structures. The IR spectra of complexes **1**−**3** (Figure 2) show absorption peaks at 1545−1542 cm^{-1} and 1427−1418 cm^{-1} that identify the antisymmetrical and symmetrical stretching vibrations of the *syn-syn* 1,3-bridging acetate.[42,43] All three complexes

(35) Gelasco, A.; Pecoraro, V. L. *J. Am. Chem. Soc.* **1993**, *115*, 7928–7929.
(36) Gelasco, A.; Kirk, M. L.; Kampf, J. W.; Pecoraro, V. L. *Inorg. Chem.* **1997**, *36*, 1829–1837.
(37) Bertoncello, K.; Fallon, G.; Murray, K.; Tiekink, E. *Inorg. Chem.* **1991**, *30*, 3562–3568.
(38) Mikuriya, M.; Yamato, Y.; Tokii, T. *Bull. Chem. Soc. Jpn.* **1992**, *65*, 1466–1468.
(39) Zhang, Z.; Brouca-Cabarrecq, C.; Hemmert, C.; Dahan, F.; Tuchagues, J.-P. *J. Chem. Soc., Dalton Trans.* **1995**, 1453–1460.
(40) Zhang, J. J.; Luo, Q. H.; Duan, C. Y.; Wang, Z. L.; Mei, Y. H. *J. Inorg. Biochem.* **2001**, *86*, 573–579.
(41) Miyasaka, H.; Clérac, R.; Wernsdorfer, W.; Lecren, L.; Bonhomme, C.; Sugiura, K.; Yamashita, M. *Angew. Chem., Int. Ed. Engl.* **2004**, *43*, 2801–2805.
(42) Deacon, G. B.; Phillips, R. J. *Coord. Chem. Rev.* **1980**, *33*, 227–250.
(43) Nakamoto, K. *Infrared and Raman Spectra of Inorganic and Coordination Compounds*, 5th ed.; Wiley-Interscience: New York, 1997; Part B, p 60.

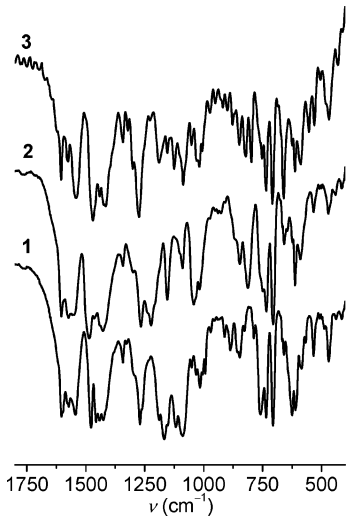

Figure 2. FT-IR spectra of complexes **1**−**3**.

exhibit strong phenolato and pyridyl absorptions between 1605 and 1575 cm^{-1} that are shifted by ≈ 10 cm^{-1} from those in the free ligands because of the coordination of the metal to these groups, and three strong bands at 611, 707, and 734 cm^{-1} attributable to non-coordinated BPh_4^-, in agreement with their molecular structure. In line with the loss of H_2O evidenced by the thermogravimetric analysis at ≈ 120 °C, compound **3** displays a broadband at ≈ 3440 cm^{-1} assigned to non-coordinated water molecules. Powdered samples of **3** and crystals of **4** show nearly identical IR spectra. The $L^{1-3(3-)}$ and $\mu_{1,3}$-carboxylato patterns are retained in the FT-IR spectra of solutions of complexes **1**−**4** in $CHCl_3$, showing that the solid state structure of these complexes is preserved upon dissolution.

ESI-Mass Spectrometry (ESI-MS). ESI-mass spectra of the complexes **1**−**3** in CH_3CN confirmed their chemical composition as well as retention of their nuclearity in solution. For complex **1**, the parent peak is observed at m/z = 709.4 (100%) in the positive mode ESI-mass spectra and originates from the $[Mn_2L^1(OAc)(OMe)]^+$ monocation. Other peaks generated during the electrospray experiments correspond to the exchange of OMe by OH ($[Mn_2L^1(OAc)(OH)]^+$, m/z = 695.4, 16%) and substitution of both exogenous bridging ligands by an oxo-bridge ($[Mn_2L^1O]^+$, m/z = 635.4, 2%). Complexes **2**−**3** afford similar mass spectra with the parent peak at m/z = 769 ($[Mn_2L^2(OAc)(OMe)]^+$) and m/z = 867 ($[Mn_2L^3(OAc)(OMe)]^+$), respectively. The isotopic patterns of these peaks match very well their simulated spectra. In addition, negative ion ESI-mass spectra of the three complexes show only one peak at m/z = 319 corresponding to BPh_4^- anion, in agreement with conductometric measurements indicating that these complexes are 1:1 electrolytes in solution.

Electronic Spectroscopy. The electronic spectra of the complexes **1**−**3** in DMF exhibit similar features (Figure 3). All three complexes show an intense absorption at 267 nm which can be attributed to intraligand π-π^* transitions. Absorptions in the 350−500 nm range correspond to L→M charge-transfer transitions from pπ orbitals of the phenoxo oxygen to the partially filled dπ orbitals of the Mn^{III} ion, as

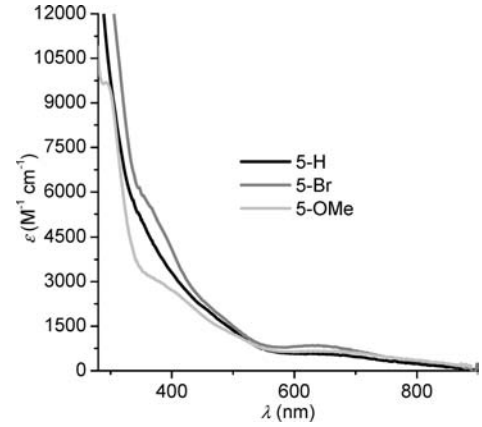

Figure 3. Electronic spectra of compounds **1**−**3**, in DMF.

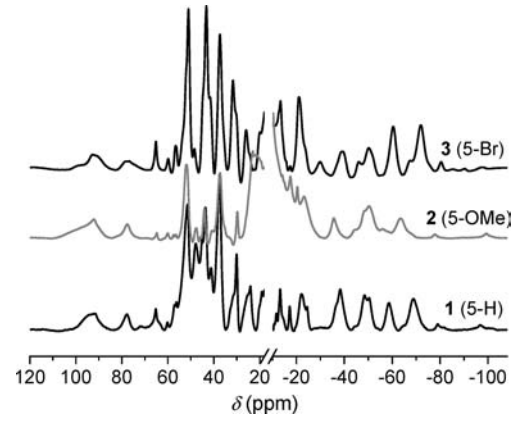

Figure 4. ^1H NMR spectra of complexes **1**, **2**, and **3** in D_6-DMSO. [catalyst] = 10 mM.

also observed for other $diMn^{III}$ complexes with phenoxo ligands.[10,11,44−47] Absorptions at 645 nm (ε = 570, 5-H), 665 nm (ε = 650, 5-OMe), and 630 nm (ε = 846, 5-Br) can be assigned to d-d transitions in agreement with reported values for related $diMn^{III}$ complexes.[44,45,48,49]

^1H NMR Spectroscopy. The paramagnetic ^1H NMR spectra of complexes **1**−**3** in D_6-DMSO show a common pattern with signals ranging from +97 to −95 ppm (Figure 4). The spectral pattern for protons of the phenol/pyridyl arms should result from a mechanism of σ/π-spin delocalization through the C bonds of the coordinated phenolato and pyridyl rings that generates large chemical shifts and relaxation values for the ring protons of the ligand.[50−53] Assuming that, like in the crystals of **4**, the d_{z^2} orbital is oriented along the $N_{py}-Mn-O_{Ac}$ bonds, the phenolato ring is expected to be predominantly influenced by a π spin-delocalization pathway

(44) Dubois, L.; Xiang, D. F.; Tan, S. S.; Pecaut, J.; Jones, P.; Baudron, S.; Le Pape, L.; Latour, J. M.; Baffer, C.; Chardon-Noblat, S.; Collomb, M. N.; Deronzier, A. *Inorg. Chem.* **2003**, *42*, 750–760.
(45) Karsten, P.; Neves, A.; Bortoluzzi, A.; Strähle, J.; Maichle-Mössmer, C. *Inorg. Chem. Commun.* **2002**, *5*, 434–438.
(46) Neves, A.; Erthal, S. M. D.; Vencato, I.; Ceccato, A. S.; Mascarehas, Y. P.; Nascimento, O. R.; Hörner, M.; Batista, A. A. *Inorg. Chem.* **1992**, *31*, 4749–4755.
(47) Hirotsu, M.; Kojima, M.; Mori, W.; Yoshikawa, Y. *Bull. Chem. Soc. Jpn.* **1998**, *71*, 2873–2884.
(48) Suzuki, M.; Mikuriya, M.; Murata, S.; Uehara, A.; Oshio, H.; Kida, S.; Saito, K. *Bull. Chem. Soc. Jpn.* **1987**, *60*, 4305–4312.
(49) Gultneh, Y.; Tesema, Y. T.; Yisgedu, T. B.; Butcher, R. J.; Wang, G.; Yee, G. T. *Inorg. Chem.* **2006**, *45*, 3023–3033.

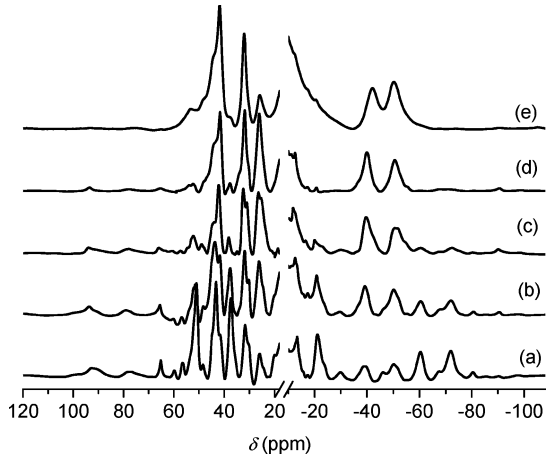

Figure 5. ^{1}H NMR spectra of **3** (10 mM), before (a) and after addition of (b) 0.5, (c) 1.0; (d) 2.0 equiv of NaOAc, and (e) 2.0 equiv of NaBzO, in D_6-DMSO.

involving molecular d_π orbitals while the pyridyl ring should be influenced by both σ and π spin delocalization involving the occupied d_{z^2} and d_π orbitals. Besides, if the two phenolato and pyridyl rings in these complexes are not in phase (or are not symmetrically related) the ^{1}H NMR signals for the two phenolato and pyridyl moieties should be observed at different positions. Consequently, sixteen (**1**) and fourteen (**2**−**3**) resonances are expected from two magnetically non-equivalent terminal pyridyl and phenolato ring protons, shifted down or upfield depending on the dominating, σ or π, spin-delocalization. Figure 4 appears to show all of these peaks (although we have not attempted to assign them) as well as the broader peaks of methylene protons spanning the full range of the spectra.[50]

For a number of Mn_2^{III}-μ-OAc complexes, the methyl group of the bridging acetato has been characterized by a broad resonance with large downfield shift.[50,54] With the aim of identifying the bridging acetato resonance, sodium acetate was added to the D_6-DMSO solution of complex **3**. Shown in Figure 5b−d are the spectra taken after addition of 0.5−2.0 equiv of acetate to the solution used to obtain the spectrum of Figure 5a. The significant points regarding the spectral pattern changes upon addition of acetate are as follows: (i) none of the signals showed the expected upfield shift as a consequence of acetate addition (if chemical exchange takes place, an upfield shift for the bridging acetato resonance is expected to be a linear function of acetate added); (ii) a lower number of resonances is now observed suggesting formation of a compound with higher symmetry. Result (i) may imply that acetate is either bound as a terminal ligand in solution with a chemical shift in the diamagnetic region or it is strongly bound and the exchange process is slow on the NMR time-scale. A slow exchange process is not surprising because bridging acetato in these complexes is not easily substituted, as shown by the formation of **4** which implies replacement of the μ-OMe bridge by a μ-OEt one with retention of μ-OAc. These points together with the analogous pattern observed for the complex treated with 2.0 equiv of Bu_4NOH or sodium benzoate (Figure 5e) suggest that it is indeed the basic medium that causes the spectral changes, most probably through conversion of the starting methoxo-bridged complex into a μ-oxo one. For this μ-oxo complex we may assume a higher symmetry than that of **3** (in accordance with the simpler spectrum (Figure 5d,e), that results in the equivalence of the two pyridyl rings as well as of the phenolato rings with the d_{z^2} orbital of the Mn atom oriented along the short Mn-*O*-oxo bond. The methoxo/oxo exchange in basic medium was confirmed by mass spectrometry. ESI-mass spectra obtained after addition of 2 equiv of Bu_4NOH over the catalyst solution, were dominated by the peak at *m*/*z* 853 belonging to the $[Mn_2L^3(OAc)(OH)]^+$ monocation. Electronic spectroscopy provided another piece of evidence supporting formation of the μ-oxo substituted complexes. UV−vis spectra of DMF solutions of complexes **1**−**3** plus 2 equiv of Bu_4NOH (or AcO^-) showed a d-d band at $\approx$ 500 nm characteristic of (μ-oxo)(μ-carboxylato)Mn^{III}_2 complexes.[55]

Kinetic Stability of the Complexes. Complexes **1**−**3** are EPR silent in the solid state and in DMF or CH_3CN frozen solution ($T \approx 117$ K), a fact consistent with the presence of Mn^{III} ions. No EPR signal was observed even after 24 h or when air was bubbled through the complex solutions. The complexes are EPR silent in the presence of water (up to 10%), meaning that water does not induce disproportionation of the Mn^{III}_2 core. The stability of complexes **1**−**3** was also checked by UV−vis spectroscopy. Spectra of the complexes registered at different time-lengths after preparation of Ar saturated solutions in anhydrous DMF or CH_3CN, even when water was added (up to 10%), showed identical λ_{max} and molar absorbance coefficients.

Electrochemical Studies. The electrochemical properties of complexes **1**−**3** were investigated by cyclic voltammetry in DMF and CH_3CN solutions containing 0.1 M Bu_4NPF_6. In DMF, the three complexes exhibit one quasi-reversible reduction wave at $E_{1/2}$ −37 mV (**1**), −115 mV (**2**), and 32 mV (**3**) (Figure 6a−c). Linear voltammetry confirmed that these waves correspond to reduction processes. $W_{1/2}$ values of 114 mV for **1**, 127 mV for **2**, and 115 mV for **3** in the square-wave voltammetry experiments suggest that this reduction corresponds to a one-electron process and may be attributed to the $Mn^{III}_2/Mn^{III}Mn^{II}$ redox couple. In the case of complexes **2** and **3**, an additional re-oxidation wave appeared at 170 mV for **2** and 300 mV for **3,** associated to the reduction wave. This extra peak could correspond to the oxidation of the chemically transformed $Mn^{II}Mn^{III}$ form of the complex. In CH_3CN, the three complexes showed a one-electron quasi-reversible reduction wave at $E_{1/2}$ −46 mV (**1**), −120 mV (**2**), and 38 mV (**3**).

(50) Wright, D. W.; Mok, H. J.; Dubé, C. E.; Armstrong, W. H. *Inorg. Chem.* **1998**, *37*, 3714–3718.
(51) Bermejo, M. R.; González, A. M.; Fondo, M.; García-Deibe, A.; Maneiro, M.; Sanmartín, J.; Hoyos, O.; Watkinson, M. *New J. Chem.* **2000**, *24*, 235–241.
(52) Pyrz, J. W.; Roe, A. L.; Stern, L. J.; Que, L., Jr. *J. Am. Chem. Soc.* **1985**, *107*, 614–620.
(53) Aromi, G.; Bhaduri, S.; Artús, P.; Huffman, J. C.; Hendrickson, D. N.; Christou, G. *Polyhedron* **2002**, *21*, 1779–1786.
(54) Hage, R.; Gunnewegh, E. A.; Niël, J.; Tjan, F. S. B.; Weyhermüller, T.; Weighardt, K. *Inorg. Chim. Acta* **1998**, *268*, 43–48.
(55) Albela, B.; Chottard, G.; Girerd, J. J. *J. Biol. Inorg. Chem.* **2001**, *6*, 430–434.

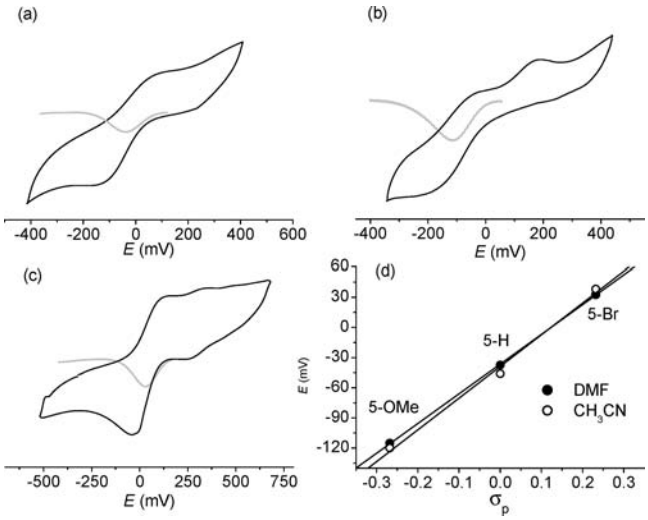

Figure 6. Cyclic (black line) and square-wave voltammogram (gray line) of (a) **1**, (b) **2**, and (c) **3**, in DMF. Conditions: Pt/Pt/Ag-AgCl; conc. = 1 mM; supporting electrolyte = Bu_4NPF_6. Scan rate (CV) = 100 mV/s. Scan frequency (SWV) = 5 Hz. (d) Hammet plot of redox potentials of complexes **1**−**3** in DMF and CH_3CN against substituent parameter, σ_p.

As expected, the substituent on the phenolato arms influences the redox potentials. Therefore, the $Mn^{III}{}_2$/$Mn^{II}Mn^{III}$ redox potential of **1**−**3** increases with the electron-withdrawing ability of the substituent, yielding a good linear correlation when plotted against the Hammett substituent constants (σ_p), as shown in Figure 6d.

On the oxidative side, **1**−**3** exhibit one irreversible wave at E_p 1.03 V (DMF) and 0.9 V (CH_3CN), corresponding to the oxidation of the free BPh_4^- anion. No metal centered oxidation is observed in the anodic scan probably because the intense oxidation wave of BPh_4^- around 1 V hides the wave corresponding to the oxidation of complexes **1**−**3** to the $Mn^{III}Mn^{IV}$ mixed valence. It is however evident that reduction and oxidation processes take place at widely different potentials yielding electrochemical stability of these complexes over a ≈ 1 V potential range. A similar overall electrochemical behavior has also been observed for the related $[Mn^{III}{}_2(\mu\text{-OAc})_2(\text{dbhbpmmpO})]^+$ complex (dbhbpmmpOH = 2,6-bis{[(3,5-di-*tert*-butyl-2-hydroxybenzyl)(2-pyridylmethyl)amino]methyl}−4-methylphenol),[56] in which each Mn possesses an N_2O_4 coordination sphere and the $Mn^{III}{}_2/Mn^{II}Mn^{III}$ and $Mn^{III}{}_2/Mn^{III}Mn^{IV}$ redox processes take place at 0.04 and 0.95 V, respectively. At variance with these complexes, $[Mn_2(\mu\text{-OAc})(\mu\text{-OMe})(\text{hbpmpnO})]^+$ (hbpmpnOH = 1,3-bis[(2-hydroxy-benzyl)(2-pyridylmethyl)amino]propan-2-ol) is stable in a narrower ΔE range (≈ 0.6 V, CH_3CN), and the $Mn^{III}{}_2/Mn^{III}Mn^{IV}$ couple is shifted to significantly lower potentials: 0.23 V.[20] Although the three types of ligands bear two N_2O_2 donor sets and the same chelating arms, they differ in the length of the spacers between the central *O*-alcoholato/phenolato and the *N*-amino donor groups: one C-atom for hbpmpnOH versus two C-atoms for H_3L^{1-3} and dbhbpmmpOH. These changes in the ligand framework modulate the oxidation potentials of the resulting $diMn^{III}$ complexes: an increase in the chelate ring size results in an increased stability of the Mn^{III} ion toward oxidation. A similar effect was observed for complexes differing only in the length of their chelating arms.[49]

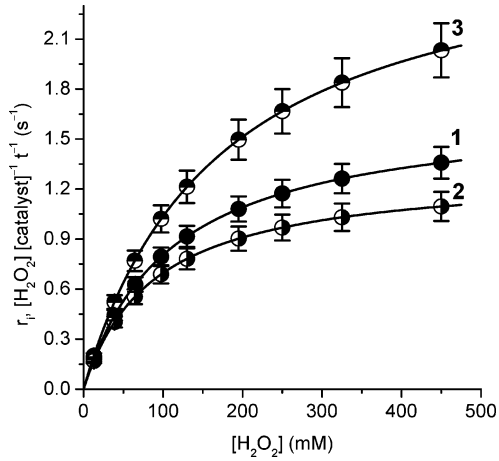

Figure 7. Effect of the $[H_2O_2]$ on the initial rate of H_2O_2 disproportionation at 10 °C, in DMF.

H_2O_2 Dismutation Studies. Stoichiometry. The ability of complexes **1**−**3** to catalyze H_2O_2 disproportion was tested in DMF, CH_3CN, and methanol. Addition of H_2O_2 to a solution of the catalyst causes an immediate vigorous evolution of dioxygen coupled to color change: from green to brown in DMF and CH_3CN, and from green to yellow in methanol. Turnovers as high as 1500 without significant decomposition were measured for the three complexes in DMF. In CH_3CN, complexes **1**−**3** were able to disproportionate up to 300 equiv of H_2O_2, while rapidly inactivated in methanol.

Kinetics. The initial rate of H_2O_2 disproportionation by complexes **1**−**3** in DMF was measured as a function of the complex and substrate concentrations at 10 °C. At constant $[H_2O_2]_0$, the initial rate of H_2O_2 disproportionation varies linearly with the [catalyst], meaning that the reaction is first-order on catalyst. At constant [catalyst], the initial rate of H_2O_2 dismutation exhibits saturation kinetics with $[H_2O_2]_0$ (Figure 7), and the experimental data could be fitted to the Michaelis−Menten equation from which the catalytic turnover number (k_{cat}) and the Michaelis constant (K_M) were determined. At 25 °C, the uncertainty on k_{cat} and K_M values is large because the reaction rate is far from its maximal value, even for 500 mM H_2O_2. This was especially evident for **3** which possess the higher K_M value. For this reason, kinetic parameters obtained at this temperature were disregarded. Values of k_{cat} and K_M obtained for complexes **1**−**3** at 10 °C in DMF are listed in Table 3 together with those of other alkoxo-bridged diMn complexes for which kinetic studies reported the k_{cat} and K_M values.

Spectroscopic Monitoring of the Catalase-Like Reaction. Room temperature UV−visible absorption spectra taken in DMF during the progress of the reaction of complexes **1**−**3** with excess H_2O_2 exhibited a new absorption band at ≈500 nm that grew in and persisted after complete consumption of H_2O_2 concurrently with the decrease and disappearance of the absorbance at 630−665 nm (shown in Figure 8 for **1**). The position and ε of the absorption band at

(56) Lomoth, R.; Huang, P.; Zheng, J.; Sun, L.; Hammarström, L.; Akermark, B.; Styring, S. *Eur. J. Inorg. Chem.* **2002**, 2965–2974.

Table 3. Kinetic Parameters for Complexes **1**−**3** and Comparison with Other Dimanganese Catalysts Including Polydentate Ligands with a Central Bridging Alcoholato[a]

catalyst	k_{cat} (s^{-1})	K_M (mM)	solvent, T (°C)	ref
1	11.69(7)	$1.1(1) \times 10^2$	DMF, 10	this work
2	1.31(5)	$8.8(9) \times 10$	DMF, 10	this work
3	2.8(2)	$1.7(2) \times 10^2$	DMF, 10	this work
$[Mn_2(\mu\text{-OAc})_2(X\text{-hbpmpnO})]^+$	3.4−23	$(1.5-6.0) \times 10^2$	DMF, 25	20
$[Mn(X\text{-salpnO})]_2$	4.2−21.9	$10-1.2 \times 10^2$	CH_3CN, 25	21
$[Mn_2(\mu\text{-O})(OAc)(OH)(benzimpnO)]^+$	2.7	6	MeOH:H_2O, 25	23
$[Mn_2(\mu\text{-OMe})(\mu\text{-OAc})(X\text{-salpentO})S_2]^+$	0.75−7.9	16−78	DMF, 25	10, 11, 17−19

[a] benzimpnOH = *N*,*N*,*N*′,*N*′-tetrakis(2-methylenebenzimidazolyl)-1,3-diaminopropan-2-ol; hbpmpnOH = 1,3-bis[(2-hydroxybenzyl)(2-pyridylmethyl)-amino]propan-2-ol; salpnOH = 1,3-bis(salicylidenamino)propan-2-ol; salpentOH = 1,5-bis(salicylidenamino)pentan-3-ol. S = solvent. X= aromatic substituents.

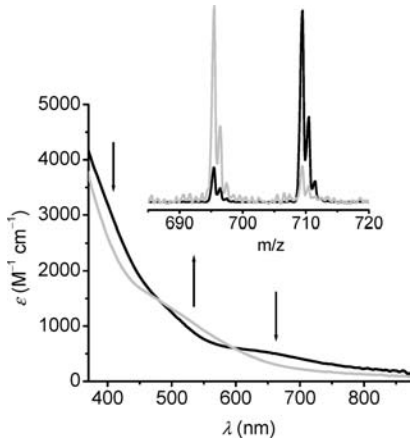

Figure 8. Electronic and ESI-mass spectra of **1** before (black line) and after (gray line) addition of 100 equiv of H_2O_2.

500 nm are comparable to those assigned to a d-d transition in (μ-oxo)(μ-carboxylato)Mn^{III}_2 complexes, and ε is clearly lower than that reported for the phenolato-to-Mn^{III} charge transfer transition.[55,57,58] The absorption band at 500 nm persisted upon successive additions of 100 equiv of H_2O_2 to the DMF solution of the catalyst, and the O_2 production rate measured after each new addition was essentially constant, indicating that the oxo-bridged species is the active form of the catalyst. Conversion of the starting complex into $[Mn_2(OAc)(O)L]$ during the reaction was confirmed by mass spectrometry. ESI-mass spectra obtained after addition of 100 equiv H_2O_2 to the catalyst solution were dominated by the peak of $[Mn_2(OAc)(OH)L]^+$ (shown for **1** (m/z = 695) in the inset of Figure 8). These results provided a clear indication that the starting Mn^{III}_2 complex converts into the $[Mn_2(OAc)(O)L]$ one during the catalytic cycle (the protonated form of which is observed in the mass spectra) and that the active form of the catalyst contains bound acetato. In CH_3CN, ESI-mass spectra taken at different reaction times showed substantial intensity decrease of the peak corresponding to $[Mn_2(OAc)(OH)L]^+$, indicating partial loss of catalyst in agreement with the lower turnover numbers observed for complexes **1**−**3** in CH_3CN. ^1H NMR spectra of 10:1 H_2O_2/catalyst reaction mixtures in D_6-DMSO obtained at the end of the reaction were identical to those obtained upon addition of 2 equiv of base (or AcO^- or BzO^-) to the solution of catalyst, indicating that the oxo-diMn species formed either during catalysis or in basic medium are essentially the same.

The EPR spectra of complexes **1**−**3** recorded in frozen DMF at various times following addition of 150 equiv of H_2O_2 were essentially EPR silent, except for a very small six-line signal at $g \approx 2$ (hyperfine splitting of ~90 G), which slowly increased for long reaction times. This signal, which includes weak doublets inserted between the six absorptions ($\Delta m = 1$ nuclear-spin-forbidden transitions characteristic of the hyperfine structure of an uncoupled Mn^{II} ion[59]), persisted and intensified upon successive additions of H_2O_2, indicating formation of an irreversible final product, and not an intermediate species. The absence of EPR signal during the reaction course, except for the inactive uncoupled Mn^{II} species, suggests that the Mn^{III}_2 form of the catalyst is the dominant species in solution since all other known forms of the diMn complexes are EPR active. The intensity of the weak 6-line signal rapidly increased upon addition of *p*-toluensulphonic acid to the reaction mixture in DMF, concomitantly to the loss of catalytic activity of the complex. Therefore, protonation of the catalyst favors formation of an inactive uncoupled Mn^{II} species, which is only a minor species when the reaction is performed in the absence of proton source (the intensity of the EPR signal of a 150:1 H_2O_2/catalyst mixture in DMF was 2−6% of that for the same reaction performed in DMF plus *p*-toluensulphonic acid). This can explain the loss of activity observed for these complexes in methanol, a protic solvent.

Discussion

Ligands H_3L^{1-3} yield complexes **1**−**4** with a triply bridged bis(μ-alkoxo)($\mu_{1,3}$-carboxylato) diMn^{III} core that are structural mimics of the Mn^{III}_2 form of Mn catalases. X-ray crystallographic data of **4**, where the methoxo is replaced by an ethoxo bridge, show that the Mn···Mn distance (2.95/6 Å) in these complexes is only 0.07−0.19 Å shorter than the Mn···Mn separation of 3.03 and 3.14 Å found in the Mn^{III}_2 form of *L. plantarum*[3] and *T. thermophilus*,[4] respectively, where the two Mn ions are triply bridged through a $\mu_{1,3}$-carboxylato and two solvent-derived single *O*-bridges. Solid state and solution spectroscopic studies indicate that the nature of the phenolato ring substituent does not affect

(57) Sheats, J. E.; Czernuszzewicz, R. S.; Dismukes, G. C.; Rheingold, A. L.; Petrouleas, V.; Stubbe, J.; Armstrong, W. H.; Beer, R. H.; Lippard, S. J. *J. Am. Chem. Soc.* **1987**, *109*, 1435–1444.
(58) Wieghardt, K.; Bossek, U.; Nuber, B.; Weiss, J.; Bonvoisin, J.; Corbella, M.; Vitols, S. E.; Girerd, J. J. *J. Am. Chem. Soc.* **1988**, *110*, 7398–7411.
(59) Bleaney, B.; Rubins, R. S. *Proc. Phys. Soc. London* **1961**, *77*, 103–112.

the coordination mode of the ligand, or the structure of the dimetallic core of complexes **1**−**3**, and that their structure is retained in methanol, CH_3CN, or DMF solution, even in the presence of water.

The three complexes catalyze dismutation of H_2O_2 with saturation kinetics on substrate (Figure 7) and first order dependence on catalyst. The lack of any pattern different from that of Mn^{III} in the electronic spectra, the retention of the dinuclearity evidenced in the ESI-mass spectra, and the absence of EPR signal during the reaction course, except for the inactive uncoupled Mn^{II} species present in very low proportion, suggest that the major active form of the catalyst occurs in the $Mn^{III}{}_2$ oxidation state during cycling: $Mn^{III}{}_2$ complexes being EPR silent, no EPR signal is expected for the catalyst in this oxidation state.

Although the substituent on the phenolato arms has negligible influence on the structure of the complexes in this series, it affects their redox potential and their catalase activity. Figure 6d and Table 3 show that the redox potentials and the catalytic activity of the complexes increase with increasing electron-withdrawing ability of the substituent, and a linear correlation results when $\log(k_{cat})$ are plotted against the redox potentials of complexes **1**−**3** (not shown), the last used as a measure of electronic effects of substituents. As a result, complex **3**, with the Br-substituent, is the best oxidant (electron-withdrawing effect stabilizes lower oxidation states) and has the highest k_{cat} among the complexes of this family. However, this complex possesses higher K_M value than the unsubstituted and 5-OMe derivatives, meaning that the electron-withdrawing group lowers the affinity of the catalyst for the substrate. Thus, although the Br derivative (**3**) is more effective at oxidizing H_2O_2 it has difficulty at binding the substrate, implying that maximal rate can only be achieved at higher $[H_2O_2]$ than for the unsubstituted (**1**) or the 5-OMe (**2**) derivatives. The fact that the catalyst which is easier to reduce reacts faster (electron-withdrawing > H > electron-donating substituent) indicates that reduction of the catalyst with simultaneous H_2O_2 oxidation should be the slow step in the catalytic cycle. This implies that the oxidized form of the catalyst is the major catalytic species in solution, which, from the spectroscopic studies, is a $Mn^{III}{}_2$ species. Therefore, kinetic and spectroscopic results converge at a catalytic cycle that runs between $Mn^{III}{}_2$ and $Mn^{II}{}_2$ oxidation states, which are the oxidation states of Mn in the MnCAT catalytic cycle.[4] Oxidation of the reduced form of the catalyst should occur in a fast step within the catalytic cycle thus preventing its spectroscopic observation.

In DMF, catalysts **1**−**3** disproportionate more than 1500 equiv of H_2O_2 with only slight decrease of activity. However, when the reaction is performed in CH_3CN, these complexes lose activity after 300 turnovers, and in methanol (or when an acid is added to the reaction mixture in DMF) the [catalyst] rapidly decreases, activity is lost, and Mn^{2+} accumulates in the reaction mixture. It is likely that the bridging ligands of the complexes serve as internal bases facilitating deprotonation of the peroxide coupled to the redox reaction. Therefore, in the protic MeOH solvent (α_{MeOH} = 0.93),[60] or upon addition of acid to the reaction in DMF, protonation of these bridges results in the inactivation of the catalyst; in DMF, a non protic solvent (α_{DMF} = 0), these catalysts disproportionate H_2O_2 with only minute loss of activity. In CH_3CN, a solvent with intermediate proton donor ability (α_{CH3CN} = 0.19), complexes **1**−**3** show moderate activity, disproportionating up to 300 equiv of H_2O_2.

Scheme 1. Proposed Catalytic Cycle for the H_2O_2 Disproportionation by Complexes **1**−**3**

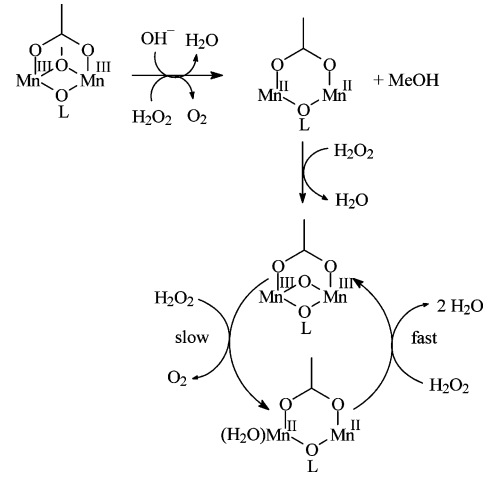

Spectroscopic monitoring of catalyzed H_2O_2 disproportionation revealed that the starting complex converts into a new species that retains bound acetate, while the methoxo bridge is replaced by an oxo one. This species dismutates H_2O_2 at constant rate upon successive additions of H_2O_2, suggesting that it is the true catalyst. The first order dependence of the reaction rate on catalyst and the lack of time-lag at the onset of the reaction suggest that the starting μ-methoxo-$Mn^{III}{}_2$ complex reacts with H_2O_2 at a rate comparable to that of the active μ-oxo-$Mn^{III}{}_2$ complex involved in the catalytic cycle. A possible mechanism including an active μ-oxo- $Mn^{III}{}_2$ species is presented in Scheme 1. It is proposed that initial reaction of H_2O_2 with the starting complex yields O_2 and the reduced complex $[Mn^{II}{}_2(\mu\text{-OAc})L^{1-3}]$. Proton transfer from terminally bound hydroperoxide to the methoxo ligand may account for the dissociation of methanol and facilitates the release of O_2. The reduced Mn_2^{II} complex may rapidly react with H_2O_2 to yield the oxidized catalyst: $[Mn^{III}{}_2(\mu\text{-O})(\mu\text{-OAc})L^{1-3}]$. This $Mn^{III}{}_2(\mu\text{-O})(\mu\text{-OAc})$ species is the catalytic form that participates in the slow oxidative half-reaction (turnover-limiting step). Observation of substrate saturation kinetics indicates that a catalyst-peroxide adduct is formed at the turnover-limiting step, the formation of which requires a ligand-shift to free some coordination position.[61,62] Binding of peroxide to the oxidized catalyst might take place through an acetato-shift[61] with the endogenous μ-oxo-ligand acting as internal base to assist deprotonation of the terminally bound peroxide coupled to its two-electron oxidation. This results in O_2

(60) Shorter, J. *Correlation Analysis of Organic Reactivity*; Research Studies Press: New York, 1983; pp 146−153.
(61) Feig, A. L.; Lippard, S. J. *Chem. Rev.* **1994**, *94*, 759–805.
(62) Rosenzweig, A. C.; Frederick, C. A.; Lippard, S. J.; Nordlund, P. *Nature* **1993**, *366*, 537–543.

release and formation of the reduced Mn_2^{II} catalyst: $[Mn^{II}_2(\mu\text{-}OAc)(H_2O)L^{1-3}]$. The trend in K_M as a function of the aromatic substituent supports the ligand-shift in terms of the strength of the phenoxo-Mn bond: the stronger the donation from the *O*-phenolato, the weaker the Mn-acetato interaction. Thus, the derivative including an electron-donating substituent can participate in the carboxylate-shift more easily (lower K_M) than the unsubstituted or 5-Br-substituted complexes. In the fast reductive half-reaction, the reduced Mn^{II}_2 catalyst reacts with another H_2O_2 molecule to yield H_2O and restore $[Mn^{III}_2(\mu\text{-}O)(\mu\text{-}OAc)L^{1-3}]$, thus closing the cycle. This mechanistic scheme is fully consistent with the kinetic and spectroscopic studies of H_2O_2 disproportionation by complexes **1**−**3**.

Three other classes of alkoxo-bridged diMn complexes display catalase activity by redox cycling between Mn^{III}_2 and Mn^{II}_2 oxidation states.[20,21,23] These complexes contain polydentate ligands derived from 1,3-diaminopropan-2-ol that modulate the Mn···Mn separation to ≈ 3.2−3.3 Å, and possess $Mn^{III}_2(\mu\text{-}OR)_2^{4+}$, $Mn^{III}_2(\mu\text{-}O)(\mu\text{-}OR)(OH)(OAc)^{+}$, or $Mn^{III}_2(\mu\text{-}OAc)_2(\mu\text{-}OR)^{3+}$ cores with the remaining coordination sites of the two Mn ions occupied by donor atoms of the ligand. These compounds undergo ligand-shift (alkoxide-[21] or carboxylate-shift[20]), as in the case of **1**−**3**, or possess one labile position,[23] thus offering a terminal coordination site to H_2O_2, which is then oxidized to O_2 concomitantly with reduction of the catalyst to the Mn^{II}_2 form. These three classes of complexes disproportionate H_2O_2 with saturation kinetics (entries 4−6 of Table 3), and the reported k_{cat} values are similar to those of complexes **1**−**3** (it should be noted that kinetic studies for complexes **1**−**3** were performed at 10 °C while the other complexes in Table 3 were studied at 25 °C and, in two cases, in different solvents). These values are significantly higher than k_{cat} obtained for complexes possessing $Mn_2(\mu\text{-}OAc)_2^{2+}$ or $Mn_2(\mu\text{-}OPh)_2^{2+(or\ 4+)}$ cores (0.02−0.2 s^{-1}).[16] K_M values in Table 3 also reflect the relative affinity of the alkoxo-bridged catalysts for the substrate: complexes with one labile position > complexes undergoing alkoxide-shift > complexes undergoing carboxylate-shift. At variance with these compounds, another family of alkoxo-bridged diMn complexes employs the Mn^{III}_2/Mn^{IV}_2 couple to dismutate H_2O_2.[10,11,17−19] Complexes of this family contain polydentate Schiff-base ligands derived from 1,5-diaminopentan-3-ol that modulate the intermetallic distance to 2.91−2.94 Å, possess a $Mn^{III}_2(\mu\text{-}OAc)(\mu\text{-}OR)_2^{3+}$ core with two labile coordination sites in *cis*-position to each other, and dismutate H_2O_2 with saturation kinetics (bottom entry in Table 3). Although the redox potentials of these later compounds fall in the same range as those of complexes of the other three classes, the H_2O_2 disproportionation cycle involves interconversion between the Mn^{III}_2 and $[Mn^{IV}{=}O]_2$ forms. In this case, both the short Mn···Mn separation and the occurrence of two labile coordination sites might facilitate the μ-bridging mode of peroxide leading to O−O cleavage and formation of the $[Mn^{IV}{=}O]_2$ form of catalyst. This is not possible for complexes **1**−**3** because, despite the short Mn···Mn distance (2.95/2.96 Å), saturation of the coordination sphere of the Mn ions by nonlabile donors enforces peroxide to bind Mn as a terminal ligand (through ligand-shift) resulting in a catalytic cycle that involves the Mn^{III}_2/Mn^{II}_2 couple. Thus, terminal coordination of peroxide to the Mn^{III}_2 catalyst should be the key for O_2 evolution and metal reduction observed for catalysts with none or one labile position in the Mn^{III}_2 form. This general feature should be considered to delineate new catalase models that employ the Mn^{III}_2/Mn^{II}_2 cycle in the future.

Acknowledgment. We thank the National University of Rosario, CONICET, and the National Agency for Sciences Promotion for financial support, and CONICET and CNRS for a bilateral agreement (Res.709/2005). H.B. thanks the France Embassy, Paul Sabatier University (Toulouse III) and MCyT-Argentina for fellowships. We thank Alejandro J. Vila for the use of the NMR spectrometer. The Bruker Avance II 600 MHz NMR spectrometer at Rosario was purchased with funds from ANPCyT (PME2003-0026) and CONICET.

Supporting Information Available: Crystallographic data in CIF format. This material is available free of charge via the Internet at http://pubs.acs.org.

IC8019793